Tau overload associated insufficient lysosomal hydrolysis activity through deacidification of lysosomes

Chao-Yuan Ye
Tongji Medical College of Huazhong University of Science and Technology: Huazhong University of Science and Technology Tongji Medical College

Peng Zeng
Hengyang Medical College: University of South China

Yuan-Cheng Liu
Tongji Medical College of Huazhong University of Science and Technology: Huazhong University of Science and Technology Tongji Medical College

Yan Shi
Hunan Normal University

Gong-Ping Liu
Tongji Medical College of Huazhong University of Science and Technology: Huazhong University of Science and Technology Tongji Medical College

Jian-Zhi Wang
Tongji Medical College of Huazhong University of Science and Technology: Huazhong University of Science and Technology Tongji Medical College

Xin-Wen Zhou
Tongji Medical College of Huazhong University of Science and Technology: Huazhong University of Science and Technology Tongji Medical College https://orcid.org/0000-0003-1357-7039

Qing Tian (tianq@hust.edu.cn)
Tongji Medical College of Huazhong University of Science and Technology: Huazhong University of Science and Technology Tongji Medical College https://orcid.org/0000-0003-2795-363X

Research Article

Keywords: tau, lysosome, deacidify, V-ATPase

Posted Date: August 31st, 2023

DOI: https://doi.org/10.21203/rs.3.rs-3294833/v1

Abstract

Neuronal tau overload and lysosomal dysfunction are two pathological features in Alzheimer's disease. Here, by ultra-high-resolution-fluorescence imaging and ultrastructural imaging, the lysosomes were observed larger in size, less numerous, perinuclear distributed and inhomogeneous in electron density in tau overloaded neurons of mice and tau overexpressed HEK293 (HEK293tau) cells. In these lysosomes there existed lots of accumulations and less active hydrolases, which was further confirmed by an elevated lysosomal pH and decreased levels of fluorescence-labeled hydrolysate inside lysosomes in living HEK293tau cells. The assembly of vacuolar-type proton-pumping ATPases (V-ATPases) on lysosomal membrane is crucial for maintaining the acidity of lysosome. Although the proteome and Western blotting data showed increased V-ATPase subunits in HEK293tau cells, we detected the abnormal binding of ATP6V1B2, an important V-ATPase subunit, to tau. It was suggested tau overload might destabilize lysosomal pH by binding with ATP6V1B2 and blocking V-ATPases assembly on the lysosomal membrane.

Introduction

Alzheimer's disease (AD), as the most common cause of neurodegenerative dementia, is one of the top medical care concerns across the world. AD has two defining hallmarks, namely deposition of amyloid-β (Aβ) outside neurons and overloaded abnormal tau protein aggregation into paired helical filaments and neurofibrillary tangles (NFTs) inside neurons [1, 2]. Familiar AD patients carry mutations in presenilin and amyloid precursor protein resulting in increased production of Aβ, particularly $A\beta_{40}$ and $A\beta_{42}$. The severity of sporadic AD is characterized by the progressing deposition of NFTs along a unidirectional pathway of olfactory cortex-temporal lobe-hippocampus [3]. Tau overload in brain was evident many years before clinical symptoms appeared [4] and the extent of cerebral tau lesions was related to the severity of dementia in AD patients clinically [5]. As it results in neuronal dysfunction, synaptic loss, and neurodegeneration, all of which manifest as clinical cognitive impairment, tau overload has been identified as a key pathological factor in AD progression [6, 7]. However, the roles of tau overload are not fully understood.

Lysosome is a single-membrane organelle filled with acidic hydrolases [8, 9]. As the degradation hub of the cell, it responds quickly to various signals inside and outside cell, aiming to reduce damage to cell or avoid cell death. During this process, lysosome exhibits a series of characteristic reactions, known as lysosomal stress response (LSR), including increased lysosomal pH, increased lysosome size, membrane permeabilization, cationic efflux, repositioning intracellularly, misfolded protein aggregation, cholesterol accumulation, redox catastrophe, and bioenergetic crisis [10]. In brains of AD patients, enlarged deacidified lysosomes have been observed in neurons [11, 12]. And the increased levels of lysosomal proteases were found, which correlated with NFTs scores and tau load, and occurred in neurons containing NFTs [13–16]. Additionally, emerging genetic studies repeatedly implicate lysosomal genes as associated with increased AD risk [17]. Hence, it is important to study lysosome to further understand the tau pathogenesis of AD.

By *in vivo* and *in vitro* studies, we found the lysosomes in tau overloaded cells were larger in size, less numerous, inhomogeneous in electron density, and contained undegraded accumulations. Lysosome signal (hsa04142) was enriched by the differentially expressed proteins (DEPs) from human wild-type 2N4R (full-length) tau overexpressed HEK293 cells (HEK293tau), and 38 lysosomal DEPs included lysosomal membrane proteins, proton pump associated proteins, lysosomal enzymes, and so on. The disruption of microtubule system and deficiency of lysosomal transporters (kinesin and dynein) in HEK293tau cells were also suggested in the proteome data. Furtherly, we showed that the lysosomes in tau overloaded cells having higher pH value and less active in proteolysis *in vitro*. The assembly of vacuolar-type proton-pumping ATPases (V-ATPases) on lysosomal membrane is crucial for maintaining the acidic lysosomal cavity [18]. Although the proteome and Western blot data showed increased V-ATPase subunits in HEK293tau cells, we detected the abnormal binding of ATP6V1B2, an important subunit of cytoplasmic V1 subcomplex of V-ATPase, to tau. The overload of tau also increased the nuclear level of transcription factor EB (TFEB), an important regulatory factor for lysosomal biogenesis, but the increase in TFEB did not alter lysosomal acidity. Overall, we observed tau overload leaded to insufficient lysosomal hydrolysis activity and insufficient lysosomal acidification probably by blocking the V-ATPase complex formation on the lysosomal membrane.

Materials and Methods

Antibodies, fluorochrome and plasmids

Primary antibodies used are listed in Table 1. LysoTracker™ Red DND-99 (Cat: L7528), LysoSensor™ Yellow/Blue DND-160 (PDMPO) (Cat: L7545) and DQ™ Red BSA (Cat: D12051) were from Invitrogen (Carlsbad, CA, USA). Plasmids of human wild-type 2N4R (full-length) tau and the vectors were from our lab.

Table 1
Antibodies employed in this study and their properties

Antibody	Epitopes	mAb/pAb	Catalog numbers	RRIDs	Dilution	Source
ATP6V0A1	Total ATP6V0A1	mAb	NBP1-89342	AB_11015740	1:1500 (WB)	Novus Biologicals
ATP6V0D2	Total ATP6V0D2	mAb	ab56556	AB_940404	1:1000 (WB)	Abcam
ATP6V1E1	Total ATP6V1E1	mAb	15280-1-AP	AB_2062545	1:1000 (WB)	Proteintech
ATP6V1G1	Total ATP6V1G1	mAb	16142-1-AP	AB_2062686	1:1000 (WB)	Proteintech
ATP6V1B2	Total ATP6V1G1	mAb	15097-1-AP	AB_2243297	1:2000 (WB)	Proteintech
LAMP2	Total LAMP2	mAb	sc-18822	AB_626858	1:300 (WB); 1:50 (IF)	Santa Cruz
LAMP2	Total LAMP2	mAb	ab13524	AB_2134736	1:300 (IF)	Abcam
Galectin-3	Total Galectin-3	mAb	60207-1-AP	AB_10951109	1:1000 (WB); 1:300 (IF)	Proteintech
Cathepsin B	Pro-cathepsin B and active cathepsin B	mAb	31718	AB_2687580	1:750 (WB)	Cell Signaling Technology
Cathepsin D	Pro-cathepsin D and active cathepsin D	mAb	2284	AB_10694258	1:750 (WB)	Cell Signaling Technology
Tau5	Total tau	mAb	ab80579	AB_1603723	1:2000 (WB)	Abcam
AT100	Phosphorylated tau at Thr212/Ser214	mAb	MN1060	AB_223652	1:1000 (WB)	Thermo
TFEB	Total TFEB	mAb	13372-1-AP	AB_2199611	1:1000 (WB); 1:300 (IF)	Proteintech

Abbreviations: mAb-: monoclonal antibody, WB: Western blotting. IF: immunofluorescence

Antibody	Epitopes	mAb/pAb	Catalog numbers	RRIDs	Dilution	Source
ACTIN	Total β-actin	mAb	20536-1-AP	AB_10700003	1:8000 (WB)	Proteintech
GAPDH	Total GAPDH	mAb	G8795	AB_1078991	1:10000 (WB)	Sigma-Aldrich
Lamin B1	Total Lamin B1	mAb	ab90576	AB_2049869	1:2000 (WB)	Abcam
Abbreviations: mAb-: monoclonal antibody, WB: Western blotting. IF: immunofluorescence						

Cell culture and transfection

Mouse neuroblastoma N2a cells, human embryonic kidney 293 (HEK293) cells, human wild-type 2N4R (full-length) tau overexpressed HEK293 cells (HEK293tau) and the control (HEK293vec) cells are the existed cell lines in our laboratory in our lab. All cells were cultured in Dulbecco's modified Eagle's medium (Cat: 11965092, Gibco) containing 200 μg/mL G418 (Cat: A1720, Sigma-Aldrich) and 10% fetal bovine serum (Cat: 10099, Gibco) and kept in a humidified 5% CO_2-containing atmosphere at 37ºC. The maximum number of passages for cells were 20. The plasmids were transfected by Lipofectamine 3000 (Cat: L3000015, Invitrogen) following the instructions.

Animals

C57BL/6 mice were from SPF Biotechnology Co., Ltd (Beijing, China), and the P301S-tau transgenic mice [B6; C3-Tg (Prnp-MAPT*P301S) PS19Vle/J] were from the Jackson Laboratory (Bar Harbor, ME, USA). All mice were specific pathogen-free (SPF) raised with 4–5 mice per cage, free food and water, and a 12-h light/dark cycle with lights on. They were housed in an ambient temperature of 20–26°C and humidity of 40–70%. Mice aged 9 months were picked for the experiments. All animal manipulation in this study were approved by the Animal Care and Use Committee of Huazhong University of Science and Technology ([2019] IACUC Number: S2131).

Brain slices preparation

The mice were deeply anesthetized with isoflurane and perfused with 4% cold paraformaldehyde (PFA) through the left ventricle after an initial flush with 0.01M cold phosphate-buffered saline (PBS). The brains were taken out carefully and post-fixed in 4% PFA overnight at 4℃, followed by successive dehydration in 10%, 20% and 30% sucrose in 0.01M PBS. After being embedded in optimal cutting temperature (OCT) (Cat: 4583, Sakura Finetek), the brains were cut into 30-μm-thick sections coronally by cryostat microtome (Leica CM 1950, Germany). The slices were kept in phosphor-glycerol at 4°C for storage.

Lysosomal fluorescence imaging in living cells and hydrolysis detection

Cells were cultured on the 35 mm confocal dishes (Cat: 801001, NEST) coated with Poly-D-Lysine/Laminin (Cat: P7280, Sigma-Aldrich) and incubated with 75 nM LysoTracker for live lysosome labeling. The excitation and emission spectra of LysoTracker are 577nm and 590 nm. Cells were observed by a confocal microscope (LZM 780, Zeiss, Germany) with an oil immersion objective (63×, 1.4-NA).

Lysosomal hydrolysis was assayed by DQ-BSA Red, a protein labeled with a fluorescent BODIPY dye. Once DQ-BSA enters lysosomes and cleaves by lysosomal proteases, there are unquenching and bright fluorescent fragments in lysosomes. After being incubated with 10 μg/mL DQ-BSA Red diluted in PBS overnight at 37°C, the cells were then incubated with Hoechest (Cat: B2261, Sigma) to mark the nuclei, two times washing with PBS before imaging. The excitation and emission spectra of DQ-BSA Red are 590 nm and 620 nm as described in the manufacturer's instructions.

Cells were imaged by a confocal microscope (LZM 800, Zeiss, Germany) with an oil immersion objective (63×, 1.4-NA). Images were analyzed by ImageJ software (Version 1.5Oi, Bethesda, MD, USA).

Lysosomal pH valuation in living cells

Cells were cultured on the 96 wells Assay Plate (Cat: 3603, Coring) and divided into six uses, five to perform the pH calibration curve and one for the measurements. Lysosomal pH value was determined by incubating the cultured cells with 1 μM LysoSensor for 5 minutes at 37℃. To obtain a pH calibration curve, cells were incubated with MES calibration buffer solution (25 mM MES, 115 mM KCl, 5 mM NaCl, and 1.2 mM $MgSO_4$, pH ranging from 3.4 to 6.9) containing 10 μM monensin (Cat: HY-N0150, MCE) and 10 μM nigericin (Cat: HY-100381, MCE). The excitation of LysoSensor is 405 nm, the fluorescence intensity of emission spectra in 460 nm and 540 nm were detected by a multifunctional microplate detector (Synergy H1, BioTek, USA). The lysosomal pH value in living cells was calculated by the ratio of emission 540/460 nm.

Immunofluorescence (IF) labeling of cultured cells and brain slices

Cells cultured on coverslips (Cat: 801008, NEST) in 12-well plates (Cat: 712001, NEST) were washed thrice with PBS for 5 minutes, fixed with 4% PFA for 20 minutes, then washed thrice with PBS containing 0.1% Triton X-100 for 5 minutes. After being ruptured membrane in PBS containing 0.5% Triton X-100 for 15 minutes, the cells were incubated in 3% BSA for 30 minutes at room temperature and then washed thrice with PBS containing 0.1% Triton X-100 for 5 minutes. The cells were incubated with the primary antibodies (Table 1) at 4°C overnight. After washing with PBS thrice for 10 minutes, PBS containing 0.3% H2O2 and 0.5% Triton X-100 were treated at room temperature for 30 minutes, then pre-incubated with 3% normal goat serum and incubated with primary antibody (Table 1). Subsequently, the cells or the brain slices were incubated with Green 488-conjugated secondary antibodies (Cat: A11055, ThermoFisher Scientific) or Red 546-conjugated secondary antibodies (Cat: A11081, ThermoFisher Scientific) for 1 hour at room temperature followed by washing for 30 minutes. Finally, an antifade solution containing DAPI

(Cat: P0131, Beyotime) was used to mark the nuclei. Images were taken by a super-resolution confocal microscope (Lightning system, STELLARIS 5 WLL, Leica, Germany) or a confocal microscope (LZM 800, Zeiss, Germany) and analyzed by ImageJ software (Version 1.5Oi, Bethesda, MD, USA).

Immunoprecipitation (IP) and Western blotting (WB)

The mice were deeply anesthetized with isoflurane and perfused with 0.01M cold PBS. The brains were dissected out as quickly as possible and frozen at -80°C. HEK293vec cells and HEK293tau cells were cultured on the 10cm dishes (Cat: 704001, NEST). The proteins of IP were extracted according to the instructions of Universal IP/Co-IP Toolkit (Magnetic Beads) (Cat: KTD104, Abbkine). The proteins of cytoplasmic and nuclei parts were extracted following the instructions of the Nuclear and Cytoplasmic Protein Extraction Kit (Cat: P0027, Beyotime).

The brain sample and cell sample were crushed by Ultrasonic Homogenizer (SCIENTZ-IID, Ningbo, China) at 4°C in 150 Mm NaCl, 50 mM Tris-HCl (pH 7.4), 10 mM NaF, 5 mM EDTA, 1 mM Na_3VOE_4, 2 mM benzamidine, and 1 mM phenylmethylsulfonyl fluoride. The extract was mixed with sample buffer (3:1, v/v) containing 200 mM Tris-HCl, 8% SDS, 40% glycerol, 40 mM dithiothreitol boiled and pH 7.6, for 10 minutes and then centrifuged at 12 000 ×g for 5 minutes at 4°C. Then added loading buffer containing β-mercaptoethanol and bromophenol blue and stored at -80°C.

The concentrations of protein were determined by a BCA Assay Kit (Cat: P0010S, Beyotime). An equal amount of total protein was electrophoresed by 8–15% sodium dodecyl sulfate-polyacrylamide gel electrophoresis and transferred onto 0.45μm nitrocellulose membranes (Amersham Biosciences, Pittsburgh, PA, USA). Following the transfer, the membranes were blocked in 3–5% non-fat milk for 45 minutes and incubated with primary antibody overnight at 4°C. Membranes were then incubated with IgG conjugated to IRDye® 800 CW (1:10 000; Li-Cor Bioscience) for 1 hour at room temperature away from light, and washed thrice with TBS-Tween-20 for 10 minutes. Finally, the membranes were visualized and quantitatively analyzed by Odyssey Infrared Imaging System (Li-Cor Bioscience, USA).

Transmission electron microscopy (TEM) imaging

After the mice were deeply anesthetized, the brains that have undergone internal fixation were taken out quickly. After precise positioning of hippocampal CA3 under an inverted ordinary microscope (SZ680, OPTEC, China), the tissue mass of 2 mm×2 mm×1 mm was taken out carefully. Special fixative for TEM imaging was used to soak tissue mass for 2 hours at room temperature, then overnight at 4°C. Subsequent ultrathin sectioning was completed in the Institute of Hydrobiology, Chinese Academy of Sciences (Wuhan, China). The ultrathin sections were observed under a TEM (HT7700, TITACHI, Japan).

Tau-associated proteome data acquisition and analysis

As previously [19], high-performance liquid chromatography (HPLC) fractionation, mass spectrometry (MS)-based quantitative proteome and an integrated approach involving isobaric tags for relative and absolute quantification (iTRAQ) labeling were used to quantify tau-associated proteome data. Extract and concentrate the proteins from HEK293tau and HEK293vec respectively, and digest them with trypsin.

After being labeled with iTRAQ-6plex reagents (the efficiency of labeling > 96%), the obtained peptides were fractionated by high-pH reversed phase HPLC. For HPLC-MS/MS analysis, the peptides dissolved in 0.1% formic acid were loaded onto a reversed-phase precolumn (Acclaim PepMap 100; Thermo Fisher Scientific, USA), and then separated by a reversed-phase analytical column (Acclaim PepMap RSLC; Thermo Fisher Scientific, USA). The resulting peptides were tested through a Q ExactiveTM Plus hybrid quadrupole-Orbitrap mass spectrometer (Thermo Fisher Scientific, USA). Then identify and quantify proteins by MaxQuant with an integrated Andromeda search engine (v.1.4.1.2), and the tandem mass spectra were searched against the UniProt human protein database. A DEPs was defined as the protein having 1.2-fold changes (> 1.20 or < 0.83 and $p < 0.05$). By the ClusterProfiler R package (version 3.12.0) [27], Gene Ontology (GO) and Kyoto Encyclopedia of Genes and Genomes (KEGG) pathway enrichment were analyzed. GO terms were divided into three categories (BP, CC, and MF) and the enrichment analysis were visualized by an online tool (http://www.bioinformatics.com.cn/). The protein-protein interaction (PPI) network was analyzed by the STRING database (version 11.5, https://string-db.org/).

Statistical analysis

Data were collected and analyzed blind. Statistical analyses were conducted by GraphPad Prism 9.0 (GraphPad Software, San Diego, CA). Data distributions were tested for normality using the D'Agostino-Pearson test. Comparisons between two groups were performed using the two-tailed Student's t-test, multiple groups were performed using one-way analysis of variance (ANOVA) followed by Tukey's test as appropriate. Significance is reported as * $p < 0.05$, ** $p < 0.01$, *** $p < 0.001$.

Results

Neuronal lysosomal volumes increased and active lysosomal hydrolytic enzymes decreased in P301S mouse hippocampi

Initially, by TEM imaging it was shown that in hippocampi of 17-month-old mice the longest diameters of some neuronal lysosomes reached 2236 nm, and the lysosomes with increased sizes often appeared near the nucleus (Figure. 1A), while in 7-month-old mice the longest diameters of hippocampal neuronal lysosomes were less than 1000 nm. It was also clearly shown that in hippocampi neuronal lysosomes of 17-month-old mice, the electron densities of large-sized lysosomes were extremely uneven and had accumulated contents inside (Figure. 1A). We assessed tau protein levels in hippocampi of 4-, 9-, 17-month-old C57BL/6 mice by WB (Figure. 1B), and observed higher ratio of phosphorylated tau (AT100 marked) in hippocampi of 17-month-old C57BL/6 mice (Figure. 1C).

As human tau is more toxic than murine tau [20], we then employed P301S mice carrying mutant human tau to characterize the effects of human tau overload on neuronal lysosomes *in vivo.* By WB, the slower migrating 64-kDa tau during electrophoresis represents the disease-associated, hyperphosphorylated, and aggregation-prone tau, while 55-kDa tau is the physiological form [21]. As shown, in the prefrontal lobe,

cortex, hippocampus, thalamus, and cerebellum of 9-month-old P301S mice, the levels of 64-kDa tau were significantly more than those in 9-month-old C57BL/6 mice (Figure. 2A). By TEM, in CA3 neurons of 9-month-old P301S mice we observed the large-sized lysosomes, in which undegraded contents accumulated and the average electron densities decreased (Figure. 2B, D). The average diameter of lysosomes in CA3 neurons of C57BL/6J mice was 686.5 ± 51.35 nm, while it was 1257 ± 102.6 nm in P301S mice (Figure. 2C). Most lysosomes in CA3 neurons of C57BL/6 mice showed darker and evener electron densities.

By IF labeling, we observed decreased numbers of neuronal lysosomes (red fluorescence) in the hippocampi of 9-month-old P301S mice (Figure. 2E). The count of neuronal lysosomes decreased to 33.6% of C57BL/6 mice in CA1, 18.7% in CA3 and 16.5% in DG, respectively (Figure. 2F). The average areas of single lysosome increased from 0.1553 ± 0.007126 μm^2 to 0.739 ± 0.0223 μm^2 in CA1 neuron, from 0.1893 ± 0.007284 μm^2 to 0.9753 ± 0.05844 μm^2 in CA3 neuron, and from 0.1833 ± 0.005239 μm^2 to 0.7083 ± 0.005897 μm^2 in DG neuron of P301S mice respectively (Figure. 2G).

Furtherly, we assessed the levels of two most abundant lysosomal proteases, cathepsin B (CTSB) and cathepsin D (CTSD). Precursor (pro-) proteases is processed to mature and active (act-) proteases after reaching the lysosome. In hippocampi of P301S mice, the levels of pro-CTSB and pro-CTSD were higher than those of C57BL/6 mice, while the levels of act-CTSB, act-CTSD were significantly lower (Figure. 2H and I).

Lysosomes in human tau overloaded cells were larger in size, less in number and perinuclear distributed

To get more details of the lysosomes in human tau overloaded cells, we used HEK293tau cells stably overexpressing human wild-type 2N4R (full-length) tau and control HEK293vec cells lacking tau, and marked the lysosomes in the fixed cells by LAMP2 labelled IF and performed 3D imaging (Figure. 3A). We found the total number of lysosomes in HEK293vec cells was approximately twice that of HEK293tau cells (Figure. 3C). By counting the lysosomes with different volumes, we observed the proportion of lysosomes with a volume of 0.02–0.04 μm^3 decreased significantly, while the proportion of lysosomes with a volume of 0.08–0.12 μm^3 increased significantly in HEK293tau cells (Figure. 3B). There was no difference in the total surface area of all lysosomes between two types of cells (Figure. 3D). However, the total volume of all lysosomes of HEK293tau cells increased to 32.19 ± 3.095 μm^3 (Figure. 3E), resulting in a significant decreased ratio of total surface area to total volume of intracellular lysosomes (12.27 ± 0.6691 μm^{-1}) (Figure. 3F). Also, we measured the straight line distances between the lysosomes and the edge of the nuclear, and found the lysosomes in HEK293tau cells were distributed much nearer the nucleus (Figure. 3G). LysoTracker Red-based live lysosome labeling technology was also used to observe the of lysosomes in HEK293tau and HEK293vec cells (Figure. 3H). The count of LysoTracker Red fluorescence labelled live lysosomes in one HEK293tau cells were significantly less than that in a HEK293vec cells (Figure. 3I). The average fluorescence area was 0.2135 ± 0.02932 μm^2 in HEK293vec cells, which increased by 174.7% to 0.5857 ± 0.06654 μm^2 in HEK293tau cells (Figure. 3J). In HEK293tau cells the total area of LysoTracker Red fluorescence labelled live lysosomes per cell increased by 32.6%

(Figure. 3K). These changes in the number and volume of lysosomes were also observed in human wild-type 2N4R(full-length) tau transiently transfected N2a cells (N2a-tau) (Figure. 3L-O). All these results showed that the lysosomes in tau overloaded cells were larger in size, less in number, and located closer to the nucleus.

Lysosomes in living HEK293tau cells were deacidified and less active in proteolysis

We further investigated whether the lysosomes with altered morphological characteristics in HEK293tau cells have undergone changes in degradation function. The degradation function of lysosomal proteases was assessed by DQ™ Red BSA. In HEK293vec cells, about 70% of the green spots (lysosomes) also had the red fluorescence (Figure. 4A and B). While in HEK293tau cells, only about 35% of the green spots had the red fluorescence, indicating reduced lysosomal hydrolysis. The activation of hydrolytic enzymes in lysosome is influenced by the pH value in lysosome cavity. By LysoSensor, we detected that the lysosomal pH in living HEK293vec cells was 4.76 ± 0.29, while in the HEK293tau cells the lysosomal pH was 5.147 ± 0.13 (Figure. 4C). The levels of pro-CTSB and pro-CTSD were increased in HEK293tau cells, while the act-CTSB, act-CTSD levels were significantly decreased (Figure. 4D and E). Galectin-3 (Gal3), a β-galactoside binding cytosolic lectin, is a marker of dysfunctional lysosomes [22]. In HEK293tau cells, the level of Gal3 was significantly up-regulated (Figure. 4F and G). The number of Gal3 (red fluorescence) positive lysosomes in HEK293tau cells was approximately 2.5-fold more than in HEK293vec cells (Figure.4H and I). All these data indicated an increased number of lysosomes with impaired hydrolysis ability and insufficient acidification in HEK293tau cells.

Lysosome pathway was one most enriched signaling pathway in HEK293tau cells

Through proteome technology, we investigated the cellular signaling pathways disturbed by human tau overload in cells. A total of 5045 proteins were quantified and 1432 DEPs were obtained (setting quantification fold change ≥ 1.2 and ≤ 0.83, and p-value < 0.05) including 743 up-regulated and 689 down-regulated proteins. By KEGG pathway enrichment study, the top 8 enriched pathways were dopaminergic synapse (hsa04728), phagosome (hsa04145), aminoacy-tRNA biosynthesis (hsa00970), protein processing in the endo-plasmic reticulum (hsa04141), carbon metabolism (hsa01200), lysine degradation (hsa0310), peroxisome (hsa04146) and lysosome (hsa04142) (Fig. 5A). As shown, 38 lysosomal DEPs contained four lysosomal membrane proteins (LAMP1, LAMP2, CD63 and SCARB2), four lysosomal transmembrane proteins (TMEM9, TMEM55B, TMEM106B and TMEM192), nine V-ATPase complex subunits (ATP6V0A1, ATP6V0C, ATP6V0D1, ATP6V1B2, ATP6V1C1, ATP6V1E1, ATP6V1G1, ATP6V1H and ATP6AP1), three lysosomal proteases (CTSA, CTSB, and CTSD), one lysosomal acid endonuclease (DNASE2), one lysosomal acid phosphatase (ACP2), one lysosomal ceramidase (ASAH1), one fucosidase (FUCA1), two galactosidases (GLA and NAGA), one sulfatase (GNS), two hexosaminidases (HEXA and HEXB), one mannosidase (MAN2B1), six lysosomal lipid metabolism-related molecules (ABCA2, NPC1, NPC2, PSAP, PPT1, and PPT2) and two transporters (IGF2R and CLTB)

(Figure. 5B). LAMP1, CTSD, LAMP2, GNS, PSAP, NPC2, HEXA, ATP6V1B2, ATP6V0D1, ATP6V1H, ATP6V0A1, ATP6V0C and NPC1 were the 13 core proteins (Figure. 5C). By WB, the up-regulated levels of ATP6V0A1, ATP6V0D2, ATP6V1E1, ATP6V1G1 were detected in HEK293tau cells (Figure. 4D and E).

Additionally, the abnormalities of the cytoskeletal system in HEK293tau cells were suggested by the dysregulated cytoskeleton-associated proteins (CGN, MAPRE2, EML3, ACTR8, TUBB6, TUBB2B, TUBGCP2, TUBGCP3, TBCE, TBCD, RMDN3 and TUBB) (Figure. 5F) and the down-regulated kinesin and dynein related proteins (KLC1, KIF2A, KIF4A, KIF5B, KIF7, KIF11, KIF14, KIF22, KIF23, DNAAF5, DYNC1H1, DYNC1I2, DYNC1LI2 and DYNC2H1) (Figure. 5G).

Abnormal binding of ATP6V1B2 to tau in HEK293tau cells

The acidic environment required to activate lysosomal enzymes depends on V-ATPases on the lysosomal membrane. TFEB is a master regulator of the lysosomal biogenesis including V-ATPase subunits. The abnormality of TFEB in tau overloaded cells was indicated by TFEB-related DEPS in this study (Figure. 6A). The subcellular localization of TFEB is regulated by the mechanistic target of rapamycin (mTOR)-mediated phosphorylation on Ser122, Ser142 and Ser211 to enable cytoplasmic sequestration partially via interaction with 14-3-3 [23, 24]. It is dephosphorylated by the phosphatase protein phosphatase 2A (PP2A) and then translocated to the nucleus to induce the transcription of target genes. Depletion of either the catalytic (PP2CA and PP2CB) subunit or regulatory (PP2R2A) subunit of PP2A abolished TFEB activation in response to sodium arsenite [25]. In addition, tuberous sclerosis complex 2 (TSC2) deficiency was reported to increase TFEB nuclear localization and activition with decreased TFEB phosphorylation at Ser142 and Ser 211 [26]. Our proteome results showed the down-regulated mTOR, 14-3-3 and TSC2, and up-regulated PP2R2A and PP2CA in HEK293tau cells (Figure. 7A). By WB (Figure. 6B and C) and high-resolution imaging (Figure. 6D-F), the total TFEB level and the nuclear TFEB level in HEK293tau cells were higher than those in HEK293vec cells. In the hippocampus of 9-month-old P301S mice, the total TFEB level was higher too (Figure. 6G and H). In HEK293vec cells, we observed significant increases in total and nuclear levels of TFEB at 36 hours after transient TFEB transfection (Fig. 6I) with unchanged lysosomal pH (Fig. 6J).

V-ATPase consists of a membrane-embedded V0 subcomplex (ATP6V0, including a, d, e, c, c' and c" subunits) and a cytoplasmic V1 subcomplex (ATP6V1, including A, B, C, D, E, F, G, and H subunits). The reversible assembly of V0 and V1 regulates V-ATPase activity and the isolated ATP6V1 and ATP6V0 complexes are autoinhibited. The mechanism by which ATP6V1 moves towards and assembles with ATP6V0 is not very clear. In a proteome study of NFTs from AD brains, ATP6V0D1, ATP6V1B2 and ATP6V1H were included in phosphorylated-tau interactome [27]. We screened out ATP6V1B2, ATP6V0D1, ATP6V1H, ATP6V0A1 and ATP6V0C as the core lysosomal DEPs in HEK293tau cells (Figure. 5C). By IP assay, it was shown ATP6V1B2, the brain isoform of ATP6V1B and crucial for the formation of ATP6V1 [28], binded to tau in HEK293tau cells (Fig. 6K), while ATP6V0A1 and ATP6V1G1 did not bind to tau. Therefore, tau might bind to ATP6V1B2 and inhibit ATP6V1 move to assemble with ATP6V0, thereby decreasing the number of the V-ATPases on the lysosomal membrane and resulting in an increase in pH and decreased activation of CTSB and CTSD in the lysosomes.

Discussion

Our research showed the insufficient lysosomal acidification induced by tau protein overload. We found the lysosomes in tau overloaded cells were larger in size, less numerous, inhomogeneous in electron density, and had kinds of accumulations in the cavities both *in vivo* and *in vitro*. By the fluorescence labeling based living cell imaging technologies, we detected an elevated lysosomal pH and decreased levels of fluorescence-labeled hydrolysate inside the lysosomes in HEK293tau cells. Although the proteome and WB data showed the increased V-ATPase subunits in HEK293tau cells, we found the abnormal binding of ATP6V1B2 to tau, which might block the V-ATPases formation on the lysosomal membrane, resulting in the insufficient lysosomal acidification and reduced activation of lysosomal hydrolases. The proteome data also showed the disruption of microtubule system and deficiency of lysosomal transporters (kinesin and dynein) in HEK293tau cells.

Human brain contains six main tau subtypes, which are 2N4R, 1N4R, 0N4R, 2N3R, 1N3R, and 0N3R. 2N4Rtau is the longest subtype and exists in the brain and cerebrospinal fluid of AD patients [29]. The P301S mutation is located in exon 10 of chromosome 17, which showed weaker ability to interact with microtubules [30]. *In vitro* P301S-tau formed smaller, more stable oligomers, and showed stronger seeding activity than the similar amount of wide type tau [31, 32], and P301S-tau was reported associated with early-onset fast progressive dementia [33]. The mice expressing human P301S-tau show progressively decreased synaptophysin immunoreactivity accompanied by microgliosis in hippocampus [34] and develop abundant filamentous tau inclusions at 5-month-old [35]. ALZ17 mice expressing the 2N4R (full-length) human tau do not exhibit filamentous tau aggregates at 18-month-old [35]. The P301L mutation of tau was found in monogenic frontotemporal lobar dementia (FTLD) patients [36].

The fluorescence labeling based high resolution imaging technologies helped us to find the deacidified lysosomes with reduced hydrolysis abilities in living HEK293tau cells. Recording the lysosomal acidity in the brain of living animals is still too difficult. In the cultured primary neurons transduced with adeno-associated virus (AAV) expressing green fluorescent protein (GFP)-human P301L-tau, decreased proteolysis activity was observed [37]. Lysosome deacidification has been implicated as a key driving factor in the pathogenesis of AD [38]. The lysosomal pH (between 4.5 and 5.0) is maintained primarily through a large protein complex lysosomal membrane, the proton pump V-type ATPase [18]. The assembly-disassembly of membrane-embedded ATP6V0 subcomplex and cytoplasmic V1 subcomplex dynamically regulates the activity of V-ATPase. The isolated ATP6V1 and ATP6V0 are autoinhibited.

The intracellular contents of tau might impact the levels of V-type ATPase subunits. In this study, human tau overload was accompanied by upregulation of ATP60A1, ATP6V0C, ATP6V0D1, ATP6V0D2, ATP6V1B2, ATP6V1E1, ATP6V1G1 and ATP6V1H in HEK293tau cells. Tau protein may interact with V-type ATPase subunits. In a proteome study of NFTs from AD brains, ATP6V0D1, ATP6V1B2 and ATP6V1H were identified as the interacting proteins in phosphorylated-tau interactome [27]. A multi-omics study of late-onset AD brains reported *ATP6V1A* gene and *ATP6V1B2* gene down-regulated across disease stages, and the authors identified *ATP6V1A* as a key regulator of a top-ranked neuronal subnetwork [39]. In this

study, ATP6V1B2, ATP6V1E1, ATP6V1G1, ATP6V1H, ATP6V0A1, ATP6V0C, ATP6V0D1 and ATP6V0D2 were upregulated in HEK293tau cells. ATP6V1B2 was shown bind to tau in HEK293tau cells, while ATP6V0A1 and ATP6V1G1 did not bind to tau. In a recently published study, Co-IP analysis of homogenates from HEK293T cells co-expressing EGFP-ATP6V1B2 and either HA-wide type tau or HA-S396A and S404A mutant tau showed that S396 and S404 phosphorylated tau interacted with ATP6V1B2 and impaired the function of V-ATPase. The residues 120–172 of ATP6V1B2 was suggested the tau-interaction domain [37]. In addition, this group also reported V-ATPase activity was impaired by Aβ-binding to ATP6V0C [37]. All these indicated tau-ATP6V1 binding impaired the assembling of the V-ATPases on the lysosomal membrane, resulting in lysosome deacidification. In addition, HEK293tau cells had more Gal3 positive lysosomes, indicating the lysosomes with lysosomal membrane permeabilization (LMP), a pathological condition leading to the translocation of intralysosomal components to the cytoplasm, such as H^+ and cathepsins [40].

Enlarged deacidified lysosomes have been observed inside neuron well before Aβ deposition outside neuron in AD brain [11, 12]. Here, we showed the enlarged deacidified lysosomes in tau overloaded cells both *in vivo* and *in vitro*. The volume of lysosome is regulated by the dynamic lysosomal division and fusion [41]. Ca^{2+} release from the lysosome and phosphatidylinositol (PIP) signaling at the lysosome surface control the lysosomal division and fusion. Factors that affect the lysosomal membrane Ca^{2+} channel protein transient receptor potential channel mucolipin 1 (TRPML1) [42] and Na^+ channel proteins two-pore channel proteins (TPCs) [43], as well as lysosome-specific phosphatidylinositol PI(3,5) P(2) [44], will disrupt the balance of lysosomal fission and fusion. TRPML1 regulates the lysosome size by activating calmodulin (CaM), and mTOR is their downstream target. mTOR is an important protein kinase that controls cellular metabolism. It forms two different protein complexes (mTORCs), namely the rapamycin-sensitive mTORC1 and the rapamycin-insensitive mTORC2. Increasing mTORC1 limited lysosomal enlargement induced by TRPML1 and CaM inhibition [45]. Recently, active mTORC1 was reported block lysosomal degradation of extracellular proteins by promoting ATP6V1 detain in the cytosol and suppressing V-ATPase mediated acidification. When mTORC1 activity declined, ATP6V1 moved to ATP6V0 to assemble active V-ATPases [18]. mTOR-mediated phosphorylation regulates the cytosolic retention of TFEB (inactive) [23, 24], which is an important transcription factor regulating lysosomal genes expression (including V-ATPase subunits genes) [46] and promote the lysosomal wastes clearance in AD animal [47, 48]. TFEB nuclear export required Ser 142 and Ser 138 nuclear phosphorylation was also mTOR-dependent [49]. In our data, mTOR was down-regulated in HEK293tau cells, while the higher total TFEB level and the nuclear TFEB level in HEK293tau cells and in the hippocampus of 9-month-old P301S mice were detected. So it is reasonable to doubt the impacts of upregulated TFEB and mTOR on lysosomes. In HEK293vec cells, lysosomal pH was found unchanged after upregulating TFEB in this study. So, upregulation of mTOR may reverse or exacerbate tau overload associated lysosomal enlargement and deacidification, which remains to be tested.

Consistent with the reports in AD patients [50, 13], our results showed the increased pro-CTSB and pro-CTSD levels but decreased activated forms of CTSB and CTSD in P301S mice and HEK293tau cells. The

up-regulated levels of proteases might be related to the increased nuclear TFEB, but their hydrolysis capacities were limited by the lysosome deacidification. The lysosomal pathway is the main pathway for tau degradation [51]. Tau is trafficked to the lysosome from the cytosol via both nonselective and selective pathways [52]. In the nonselective pathway, the cytosolic tau is first enveloped in a membrane that subsequently fuses with the lysosomal membrane to release tau into lysosomes. The selective pathway is known as chaperone-mediated autophagy (CMA). CTSB degrades Aβ and CTSD degrades both Aβ and tau [53, 52]. Therefore, whether tau and which type of tau accumulates in the lysosomes deserves further studies.

The cargos of endocytic and autophagic pathways maintain dynamic interactions with lysosomes, which requires the lysosomes to move bidirectionally along the microtubules throughout the cytoplasm [54]. This process is particularly more challenging in neurons due to the highly polarized morphology of neurons. Therefore, the normal functions of the microtubule system and transporting proteins are crucial to the distribution, morphology and function of lysosomes. The anterograde movement of lysosomes towards the microtubule plus-ends is mediated by kinesin [55, 56] and the retrograde movement of lysosomes towards the minus-ends is mediated by dynein [57, 58]. Pathological tau destroys the stability of the microtubule system, which in turn affects the distribution of lysosomes and the fusion of autophagolysosomes [51, 59]. In HEK293tau cells, the disruption of the cytoskeleton and deficiency of transporters of lysosomes (kinesin and dynein) were suggested by the proteome data. In addition, the transmembrane protein TMEM55B was reported to interact and recruit the dynein adaptor JIP4 to lysosomal membranes, thus inducing retrograde lysosomal trafficking towards the perinuclear region along microtubules [60]. The upregulated TMEM55B in proteome was corroborate with the perinuclear distributed of lysosomes in HEK293tau cells.

Abbreviations

AD: Alzheimer's disease; DEPs: Differentially expressed proteins; TFEB: Transcription factor EB; LSR: Lysosomal stress response; Aβ: Amyloid-β; PHF: Paired helical filaments; NFTs: Neurofibrillary tangles; PSEN: Presenilin; APP: Amyloid precursor protein; Tuberous sclerosis complex 2 (TSC2); Pro-CTSB: Procathepsin B; Pro-CTSD: Procathepsin D; Act-CTSB: Activated-cathepsin B; Act-CTSD: Activated-cathepsin D; PFA: Paraformaldehyde; PBS: Phosphate-buffered saline; OCT: Optimal cutting temperature; iTRAQ: isobaric tags for relative and absolute quantification; HPLC: High-performance liquid chromatography; MS: Mass spectrometry; GO: Gene Ontology; KEGG: Kyoto Encyclopedia of Genes and Genomes; PPI: Protein-protein interaction; ANOVA: Analysis of variance; Gal3: Galectin-3; mTOR: Mechanistic target of rapamycin; PP2A: Phosphatase protein phosphatase 2A; PIP: Phosphatidylinositol; TRPML1: Transient receptor potential channel mucolipin 1; TPCs: Two-pore channel proteins; CaM: Calmodulin; V-ATPase: V-type ATPase; CMA: Chaperone-mediated autophagy; mAb-: monoclonal antibody; WB: Western blotting; IF: Immunofluorescence; IP: immunoprecipitation.

Declarations

Acknowledgments

This work was supported by a grant from the National Natural Science Foundation of China (82041478). The imaging of this work was obtained in Medical sub-center of Analytical and Testing Center, Huazhong University of Science and Technology.

Funding

This work was supported by a grant from the National Natural Science Foundation of China (82041478).

Competing interests

The authors declare that there are no conflicts of interest.

Authors' contributions

QT initiated, designed and supervised the study. CY-Y conducted most of the experiments and all statistical analyses. PZ did the analysis of Proteome. YC-L performed part of the molecular biological experiments. CY-Y wrote the manuscript, and QT revised the manuscript. JZ-W, GP-L and XW-Z helped to comment on the manuscript.

Availability of data and materials

The datasets used and/or analyzed during the current study are available from the corresponding author on reasonable request.

Ethics approval and consent to participate

All animal experimental protocols and animal manipulation in this study were approved by the Animal Care and Use Committee of Huazhong University of Science and Technology.

Consent for publication

Not applicable

References

1. Azam S, Haque ME, Balakrishnan R, Kim I-S, Choi D-K (2021) The Ageing Brain: Molecular and Cellular Basis of Neurodegeneration. Front Cell Dev Biol 9:683459. 10.3389/fcell.2021.683459
2. Sharma K, Pradhan S, Duffy LK, Yeasmin S, Bhattarai N, Schulte MK (2021) Role of Receptors in Relation to Plaques and Tangles in Alzheimer's Disease Pathology. Int J Mol Sci 22(23). 10.3390/ijms222312987
3. Carroll T, Guha S, Nehrke K, Johnson GVW (2021) Tau Post-Translational Modifications: Potentiators of Selective Vulnerability in Sporadic Alzheimer's Disease. Biology (Basel) 10(10).

10.3390/biology10101047

4. Dujardin S, Commins C, Lathuiliere A, Beerepoot P, Fernandes AR, Kamath TV, De Los Santos MB, Klickstein N, Corjuc DL, Corjuc BT, Dooley PM, Viode A, Oakley DH, Moore BD, Mullin K, Jean-Gilles D, Clark R, Atchison K, Moore R, Chibnik LB, Tanzi RE, Frosch MP, Serrano-Pozo A, Elwood F, Steen JA, Kennedy ME, Hyman BT (2020) Tau molecular diversity contributes to clinical heterogeneity in Alzheimer's disease. Nat Med 26(8):1256–1263. 10.1038/s41591-020-0938-9
5. Braak H, Braak E (1991) Neuropathological stageing of Alzheimer-related changes. Acta Neuropathol 82(4):239–259. 10.1007/BF00308809
6. Arnsten AFT, Datta D, Del Tredici K, Braak H (2021) Hypothesis: Tau pathology is an initiating factor in sporadic Alzheimer's disease. Alzheimers Dement 17(1):115–124. 10.1002/alz.12192
7. Sinsky J, Pichlerova K, Hanes J (2021) Tau Protein Interaction Partners and Their Roles in Alzheimer's Disease and Other Tauopathies. Int J Mol Sci 22(17). 10.3390/ijms22179207
8. Perera RM, Zoncu R (2016) The Lysosome as a Regulatory Hub. Annu Rev Cell Dev Biol 32:223–253. 10.1146/annurev-cellbio-111315-125125
9. Ballabio A, Bonifacino JS (2020) Lysosomes as dynamic regulators of cell and organismal homeostasis. Nat Rev Mol Cell Biol 21(2):101–118. 10.1038/s41580-019-0185-4
10. Lakpa KL, Khan N, Afghah Z, Chen X, Geiger JD (2021) Lysosomal Stress Response (LSR): Physiological Importance and Pathological Relevance. J Neuroimmune Pharmacol 16(2):219–237. 10.1007/s11481-021-09990-7
11. Lee JH, Yang DS, Goulbourne CN, Im E, Stavrides P, Pensalfini A, Chan H, Bouchet-Marquis C, Bleiwas C, Berg MJ, Huo C, Peddy J, Pawlik M, Levy E, Rao M, Staufenbiel M, Nixon RA (2022) Faulty autolysosome acidification in Alzheimer's disease mouse models induces autophagic build-up of Abeta in neurons, yielding senile plaques. Nat Neurosci 25(6):688–701. 10.1038/s41593-022-01084-8
12. Yuan P, Zhang M, Tong L, Morse TM, McDougal RA, Ding H, Chan D, Cai Y, Grutzendler J (2022) PLD3 affects axonal spheroids and network defects in Alzheimer's disease. Nature 612(7939):328–337. 10.1038/s41586-022-05491-6
13. Chai YL, Chong JR, Weng J, Howlett D, Halsey A, Lee JH, Attems J, Aarsland D, Francis PT, Chen CP, Lai MKP (2019) Lysosomal cathepsin D is upregulated in Alzheimer's disease neocortex and may be a marker for neurofibrillary degeneration. Brain Pathol 29(1):63–74. 10.1111/bpa.12631
14. Lim F, Hernández F, Lucas JJ, Gómez-Ramos P, Morán MA, Avila J (2001) FTDP-17 mutations in tau transgenic mice provoke lysosomal abnormalities and Tau filaments in forebrain. Mol Cell Neurosci 18(6):702–714. 10.1006/mcne.2001.1051
15. Cataldo AM, Barnett JL, Berman SA, Li J, Quarless S, Bursztajn S, Lippa C, Nixon RA (1995) Gene expression and cellular content of cathepsin D in Alzheimer's disease brain: evidence for early up-regulation of the endosomal-lysosomal system. Neuron 14(3):671–680. 10.1016/0896-6273(95)90324-0

16. Cataldo AM, Paskevich PA, Kominami E, Nixon RA (1991) Lysosomal hydrolases of different classes are abnormally distributed in brains of patients with Alzheimer disease. Proc Natl Acad Sci U S A 88(24):10998–11002. 10.1073/pnas.88.24.10998
17. Szabo MP, Mishra S, Knupp A, Young JE (2022) The role of Alzheimer's disease risk genes in endolysosomal pathways. Neurobiol Dis 162:105576. 10.1016/j.nbd.2021.105576
18. Ratto E, Chowdhury SR, Siefert NS, Schneider M, Wittmann M, Helm D, Palm W (2022) Direct control of lysosomal catabolic activity by mTORC1 through regulation of V-ATPase assembly. Nat Commun 13(1):4848. 10.1038/s41467-022-32515-6
19. Zeng P, Su H-F, Ye C-Y, Qiu S-W, Shi A, Wang J-Z, Zhou X-W, Tian Q (2022) A Tau Pathogenesis-Based Network Pharmacology Approach for Exploring the Protections of in Alzheimer's Disease. Front Pharmacol 13:877806. 10.3389/fphar.2022.877806
20. Hernández F, Cuadros R, Ollá I, García C, Ferrer I, Perry G, Avila J (2019) Differences in structure and function between human and murine tau. Biochim Biophys Acta Mol Basis Dis 1865(8):2024–2030. 10.1016/j.bbadis.2018.08.010
21. Schaler AW, Runyan AM, Clelland CL, Sydney EJ, Fowler SL, Figueroa HY, Shioda S, Santa-Maria I, Duff KE, Myeku N (2021) PAC1 receptor-mediated clearance of tau in postsynaptic compartments attenuates tau pathology in mouse brain. Sci Transl Med 13(595). 10.1126/scitranslmed.aba7394
22. Jia J, Claude-Taupin A, Gu Y, Choi SW, Peters R, Bissa B, Mudd MH, Allers L, Pallikkuth S, Lidke KA, Salemi M, Phinney B, Mari M, Reggiori F, Deretic V (2020) Galectin-3 Coordinates a Cellular System for Lysosomal Repair and Removal. Dev Cell 52(1). 10.1016/j.devcel.2019.10.025
23. Zhu S-Y, Yao R-Q, Li Y-X, Zhao P-Y, Ren C, Du X-H, Yao Y-M (2021) The Role and Regulatory Mechanism of Transcription Factor EB in Health and Diseases. Front Cell Dev Biol 9:667750. 10.3389/fcell.2021.667750
24. Bouhamdani N, Comeau D, Turcotte S (2021) A Compendium of Information on the Lysosome. Front Cell Dev Biol 9:798262. 10.3389/fcell.2021.798262
25. Martina JA, Puertollano R (2018) Protein phosphatase 2A stimulates activation of TFEB and TFE3 transcription factors in response to oxidative stress. J Biol Chem 293(32):12525–12534. 10.1074/jbc.RA118.003471
26. Alesi N, Akl EW, Khabibullin D, Liu H-J, Nidhiry AS, Garner ER, Filippakis H, Lam HC, Shi W, Viswanathan SR, Morroni M, Ferguson SM, Henske EP (2021) TSC2 regulates lysosome biogenesis via a non-canonical RAGC and TFEB-dependent mechanism. Nat Commun 12(1):4245. 10.1038/s41467-021-24499-6
27. Drummond E, Pires G, MacMurray C, Askenazi M, Nayak S, Bourdon M, Safar J, Ueberheide B, Wisniewski T (2020) Phosphorylated tau interactome in the human Alzheimer's disease brain. Brain 143(9):2803–2817. 10.1093/brain/awaa223
28. Futai M, Sun-Wada G-H, Wada Y, Matsumoto N, Nakanishi-Matsui M (2019) Vacuolar-type ATPase: A proton pump to lysosomal trafficking. Proc Jpn Acad Ser B Phys Biol Sci 95(6):261–277. 10.2183/pjab.95.018

29. Wang Y, Mandelkow E (2016) Tau in physiology and pathology. Nat Rev Neurosci 17(1). 10.1038/nrn.2015.1
30. Delobel P, Flament S, Hamdane M, Jakes R, Rousseau A, Delacourte A, Vilain J-P, Goedert M, Buée L (2002) Functional characterization of FTDP-17 tau gene mutations through their effects on Xenopus oocyte maturation. J Biol Chem 277(11):9199–9205. 10.1074/jbc.M107716200
31. Martinez P, Patel H, You Y, Jury N, Perkins A, Lee-Gosselin A, Taylor X, You Y, Di Viana G, Huang X, Dutta S, Wijeratne AB, Redding-Ochoa J, Shahid SS, Codocedo JF, Min S, Landreth GE, Mosley AL, Wu Y-C, McKinzie DL, Rochet J-C, Zhang J, Atwood BK, Troncoso J, Lasagna-Reeves CA (2022) Bassoon contributes to tau-seed propagation and neurotoxicity. Nat Neurosci 25(12):1597–1607. 10.1038/s41593-022-01191-6
32. Maeda S, Sato Y, Takashima A (2018) Frontotemporal dementia with Parkinsonism linked to chromosome-17 mutations enhance tau oligomer formation. Neurobiol Aging 69:26–32. 10.1016/j.neurobiolaging.2018.04.014
33. Sánchez MP, García-Cabrero AM, Sánchez-Elexpuru G, Burgos DF, Serratosa JM (2018) Tau-Induced Pathology in Epilepsy and Dementia: Notions from Patients and Animal Models. Int J Mol Sci 19(4). 10.3390/ijms19041092
34. Yoshiyama Y, Higuchi M, Zhang B, Huang S-M, Iwata N, Saido TC, Maeda J, Suhara T, Trojanowski JQ, Lee VMY (2007) Synapse loss and microglial activation precede tangles in a P301S tauopathy mouse model. Neuron 53(3):337–351. 10.1016/j.neuron.2007.01.010
35. Clavaguera F, Bolmont T, Crowther RA, Abramowski D, Frank S, Probst A, Fraser G, Stalder AK, Beibel M, Staufenbiel M, Jucker M, Goedert M, Tolnay M (2009) Transmission and spreading of tauopathy in transgenic mouse brain. Nat Cell Biol 11(7):909–913. 10.1038/ncb1901
36. Gilberti N, Turla M, Alberici A, Bertasi V, Civelli P, Archetti S, Padovani A, Borroni B (2012) Prevalence of frontotemporal lobar degeneration in an isolated population: the Vallecamonica study. Neurol Sci 33(4):899–904. 10.1007/s10072-011-0865-0
37. Kim S-H, Cho Y-S, Kim Y, Park J, Yoo S-M, Gwak J, Kim Y, Gwon Y, Kam T-I, Jung Y-K (2023) Endolysosomal impairment by binding of amyloid beta or MAPT/Tau to V-ATPase and rescue via the HYAL-CD44 axis in Alzheimer disease. Autophagy 19(8):2318–2337. 10.1080/15548627.2023.2181614
38. Lo CH, Zeng J (2023) Defective lysosomal acidification: a new prognostic marker and therapeutic target for neurodegenerative diseases. Transl Neurodegener 12(1):29. 10.1186/s40035-023-00362-0
39. Wang M, Li A, Sekiya M, Beckmann ND, Quan X, Schrode N, Fernando MB, Yu A, Zhu L, Cao J, Lyu L, Horgusluoglu E, Wang Q, Guo L, Wang Y-S, Neff R, Song W-M, Wang E, Shen Q, Zhou X, Ming C, Ho S-M, Vatansever S, Kaniskan H, Jin J, Zhou M-M, Ando K, Ho L, Slesinger PA, Yue Z, Zhu J, Katsel P, Gandy S, Ehrlich ME, Fossati V, Noggle S, Cai D, Haroutunian V, Iijima KM, Schadt E, Brennand KJ, Zhang B (2021) Transformative Network Modeling of Multi-omics Data Reveals Detailed Circuits, Key Regulators, and Potential Therapeutics for Alzheimer's Disease. Neuron 109(2). 10.1016/j.neuron.2020.11.002

40. Wang F, Gómez-Sintes R, Boya P (2018) Lysosomal membrane permeabilization and cell death. Traffic 19(12):918–931. 10.1111/tra.12613
41. Davidson SM, Vander Heiden MG (2017) Critical Functions of the Lysosome in Cancer Biology. Annu Rev Pharmacol Toxicol 57:481–507. 10.1146/annurev-pharmtox-010715-103101
42. Di Paola S, Scotto-Rosato A, Medina DL (2018) TRPML1: The Caretaker of the lysosome. Cell Calcium 69:112–121. 10.1016/j.ceca.2017.06.006
43. Wang X, Zhang X, Dong X-P, Samie M, Li X, Cheng X, Goschka A, Shen D, Zhou Y, Harlow J, Zhu MX, Clapham DE, Ren D, Xu H (2012) TPC proteins are phosphoinositide- activated sodium-selective ion channels in endosomes and lysosomes. Cell 151(2):372–383. 10.1016/j.cell.2012.08.036
44. Dong X-p, Shen D, Wang X, Dawson T, Li X, Zhang Q, Cheng X, Zhang Y, Weisman LS, Delling M, Xu H (2010) PI(3,5)P(2) controls membrane trafficking by direct activation of mucolipin Ca(2+) release channels in the endolysosome. Nat Commun 1:38. 10.1038/ncomms1037
45. Yang Y, Xu M, Zhu X, Yao J, Shen B, Dong X-P (2019) Lysosomal Ca release channel TRPML1 regulates lysosome size by promoting mTORC1 activity. Eur J Cell Biol 98(2–4):116–123. 10.1016/j.ejcb.2019.05.001
46. Cui Z, Napolitano G, de Araujo MEG, Esposito A, Monfregola J, Huber LA, Ballabio A, Hurley JH (2023) Structure of the lysosomal mTORC1-TFEB-Rag-Ragulator megacomplex. Nature 614(7948):572–579. 10.1038/s41586-022-05652-7
47. Polito VA, Li H, Martini-Stoica H, Wang B, Yang L, Xu Y, Swartzlander DB, Palmieri M, di Ronza A, Lee VMY, Sardiello M, Ballabio A, Zheng H (2014) Selective clearance of aberrant tau proteins and rescue of neurotoxicity by transcription factor EB. EMBO Mol Med 6(9):1142–1160. 10.15252/emmm.201303671
48. Xiao Q, Yan P, Ma X, Liu H, Perez R, Zhu A, Gonzales E, Tripoli DL, Czerniewski L, Ballabio A, Cirrito JR, Diwan A, Lee J-M (2015) Neuronal-Targeted TFEB Accelerates Lysosomal Degradation of APP, Reducing Aβ Generation and Amyloid Plaque Pathogenesis. J Neurosci 35(35):12137–12151. 10.1523/JNEUROSCI.0705-15.2015
49. Napolitano G, Esposito A, Choi H, Matarese M, Benedetti V, Di Malta C, Monfregola J, Medina DL, Lippincott-Schwartz J, Ballabio A (2018) mTOR-dependent phosphorylation controls TFEB nuclear export. Nat Commun 9(1):3312. 10.1038/s41467-018-05862-6
50. Batkulwar K, Godbole R, Banarjee R, Kassaar O, Williams RJ, Kulkarni MJ (2018) Advanced Glycation End Products Modulate Amyloidogenic APP Processing and Tau Phosphorylation: A Mechanistic Link between Glycation and the Development of Alzheimer's Disease. ACS Chem Neurosci 9(5). 10.1021/acschemneuro.7b00410
51. Root J, Merino P, Nuckols A, Johnson M, Kukar T (2021) Lysosome dysfunction as a cause of neurodegenerative diseases: Lessons from frontotemporal dementia and amyotrophic lateral sclerosis. Neurobiol Dis 154:105360. 10.1016/j.nbd.2021.105360
52. Suire CN, Leissring MA (2021) Cathepsin D: A Candidate Link between Amyloid β-protein and Tauopathy in Alzheimer Disease. J Exp Neurol 2(1):10–15 No doi

53. Hook V, Yoon M, Mosier C, Ito G, Podvin S, Head BP, Rissman R, O'Donoghue AJ, Hook G (2020) Cathepsin B in neurodegeneration of Alzheimer's disease, traumatic brain injury, and related brain disorders. Biochim Biophys Acta Proteins Proteom 1868(8):140428. 10.1016/j.bbapap.2020.140428
54. Pu J, Guardia CM, Keren-Kaplan T, Bonifacino JS (2016) Mechanisms and functions of lysosome positioning. J Cell Sci 129(23):4329–4339. 10.1242/jcs.196287
55. Hollenbeck PJ, Swanson JA (1990) Radial extension of macrophage tubular lysosomes supported by kinesin. Nature 346(6287):864–866
56. Yao M, Qu H, Han Y, Cheng CY, Xiao X (2022) Kinesins in Mammalian Spermatogenesis and Germ Cell Transport. Front Cell Dev Biol 10:837542. 10.3389/fcell.2022.837542
57. Cabukusta B, Neefjes J (2018) Mechanisms of lysosomal positioning and movement. Traffic 19(10):761–769. 10.1111/tra.12587
58. Harada A, Takei Y, Kanai Y, Tanaka Y, Nonaka S, Hirokawa N (1998) Golgi vesiculation and lysosome dispersion in cells lacking cytoplasmic dynein. J Cell Biol 141(1):51–59. 10.1083/jcb.141.1.51
59. Rodríguez-Martín T, Cuchillo-Ibáñez I, Noble W, Nyenya F, Anderton BH, Hanger DP (2013) Tau phosphorylation affects its axonal transport and degradation. Neurobiol Aging 34(9):2146–2157. 10.1016/j.neurobiolaging.2013.03.015
60. Willett R, Martina JA, Zewe JP, Wills R, Hammond GRV, Puertollano R (2017) TFEB regulates lysosomal positioning by modulating TMEM55B expression and JIP4 recruitment to lysosomes. Nat Commun 8(1):1580. 10.1038/s41467-017-01871-z

Figures

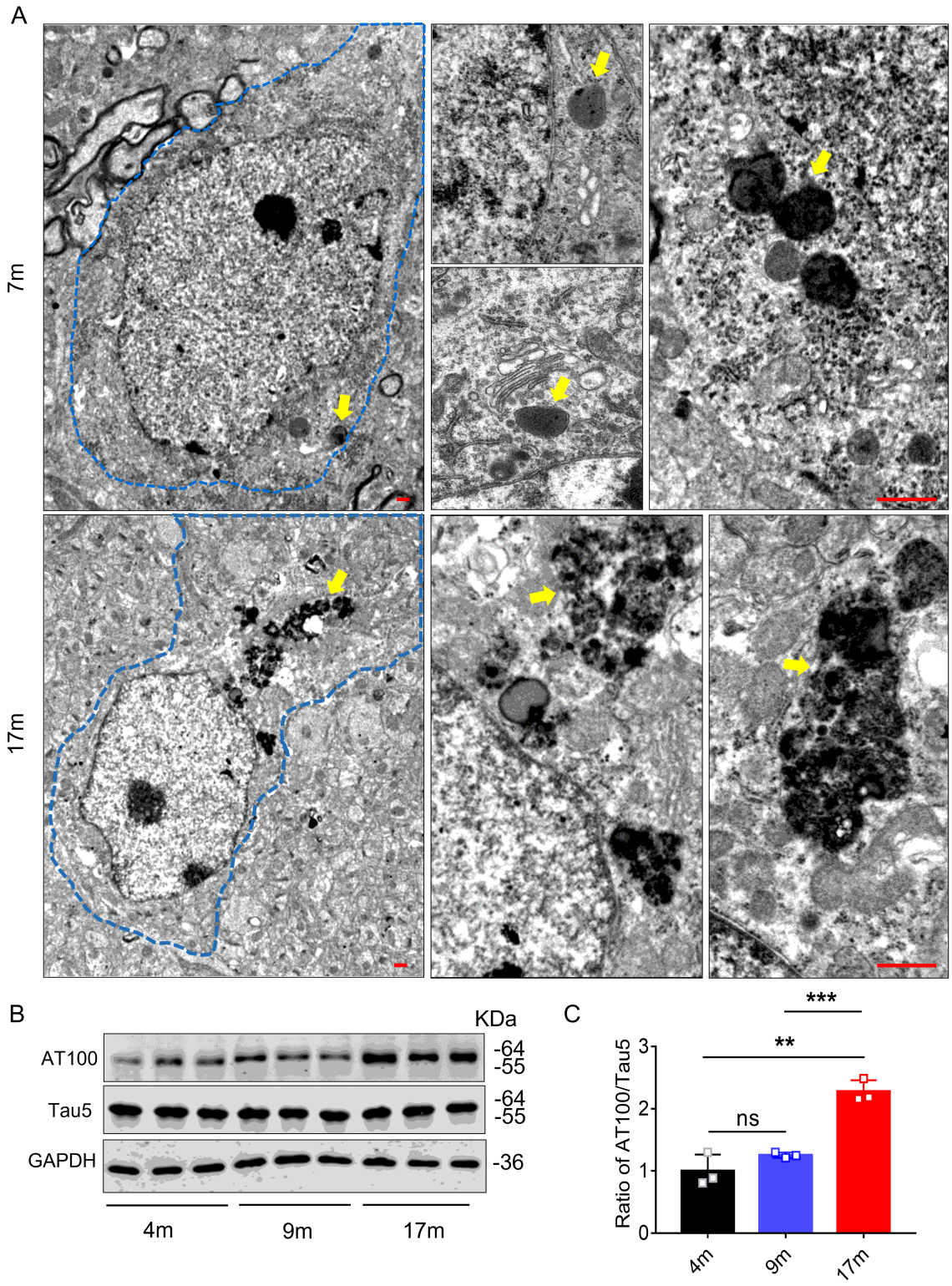

Figure 1

Legend not included with this version.

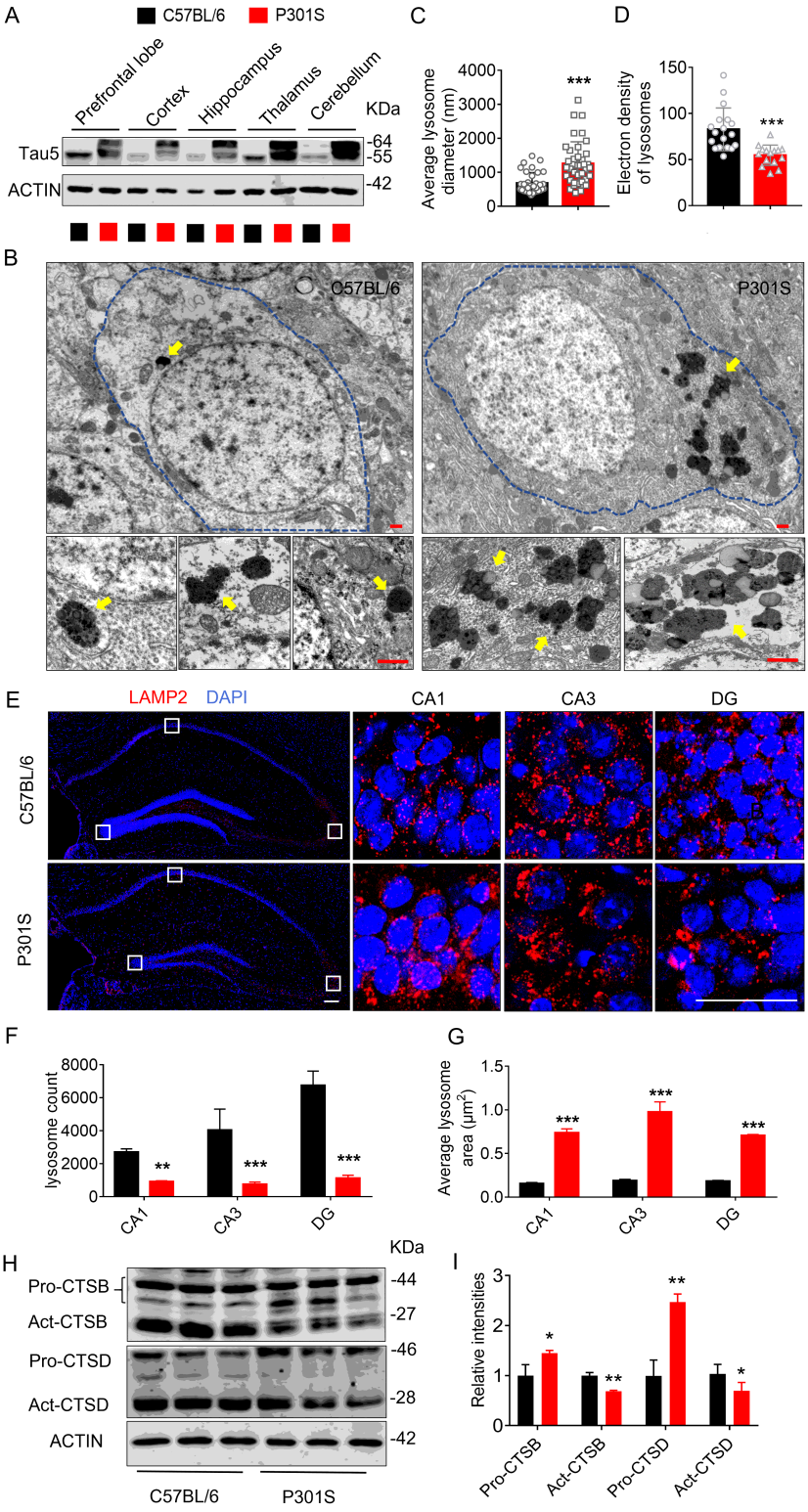

Figure 2

Legend not included with this version.

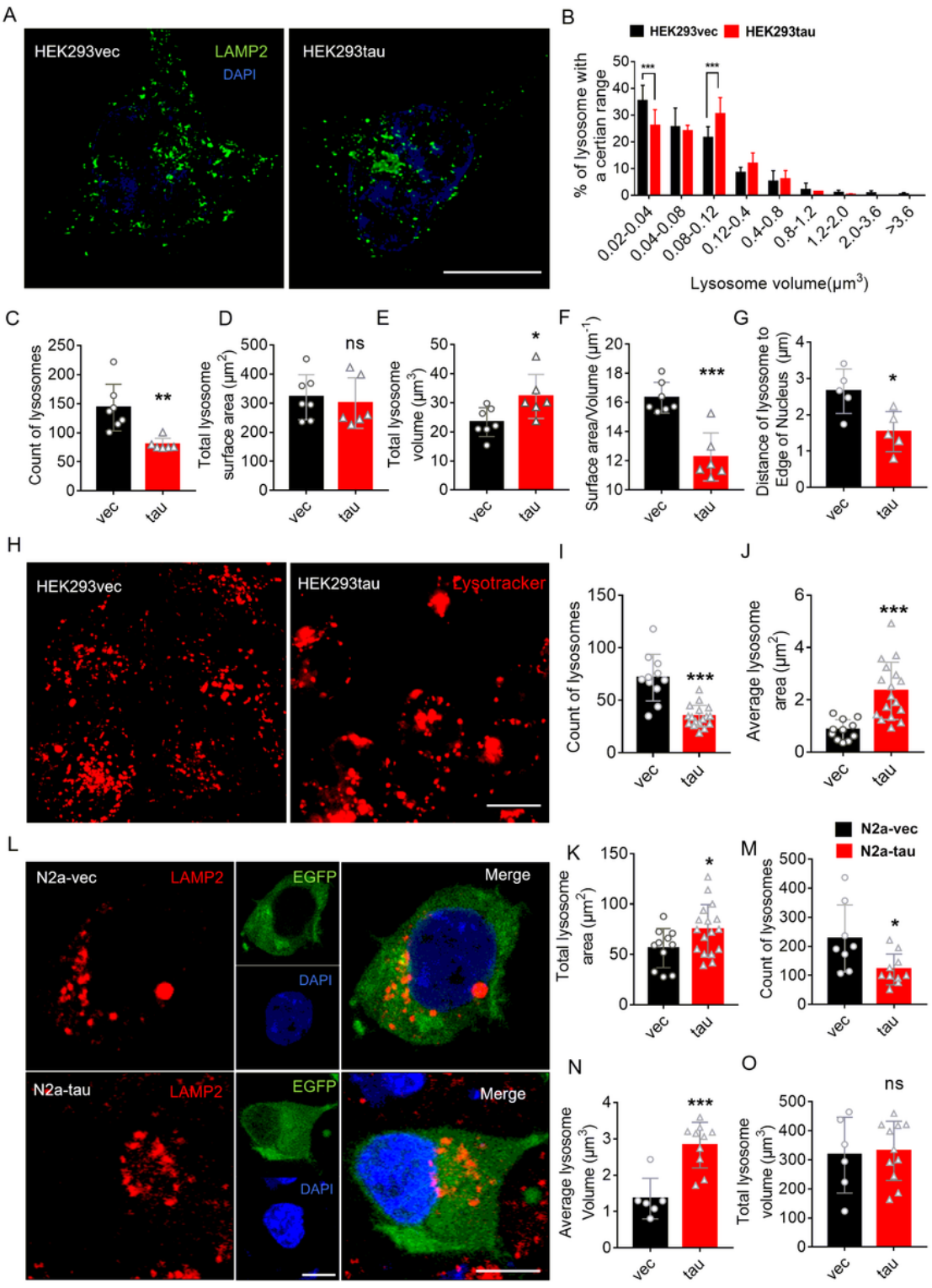

Figure 3

Legend not included with this version.

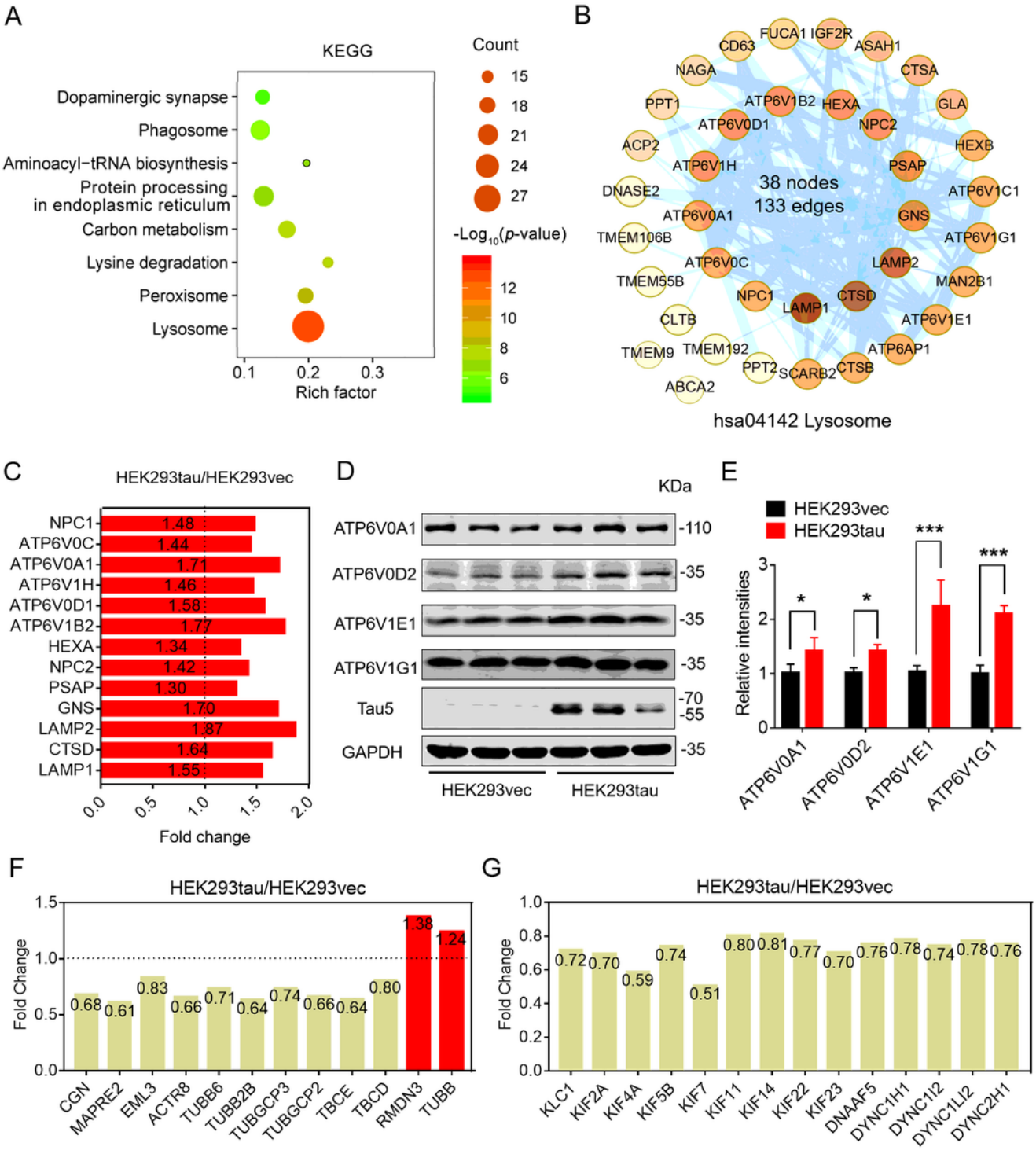

Figure 4

Legend not included with this version.

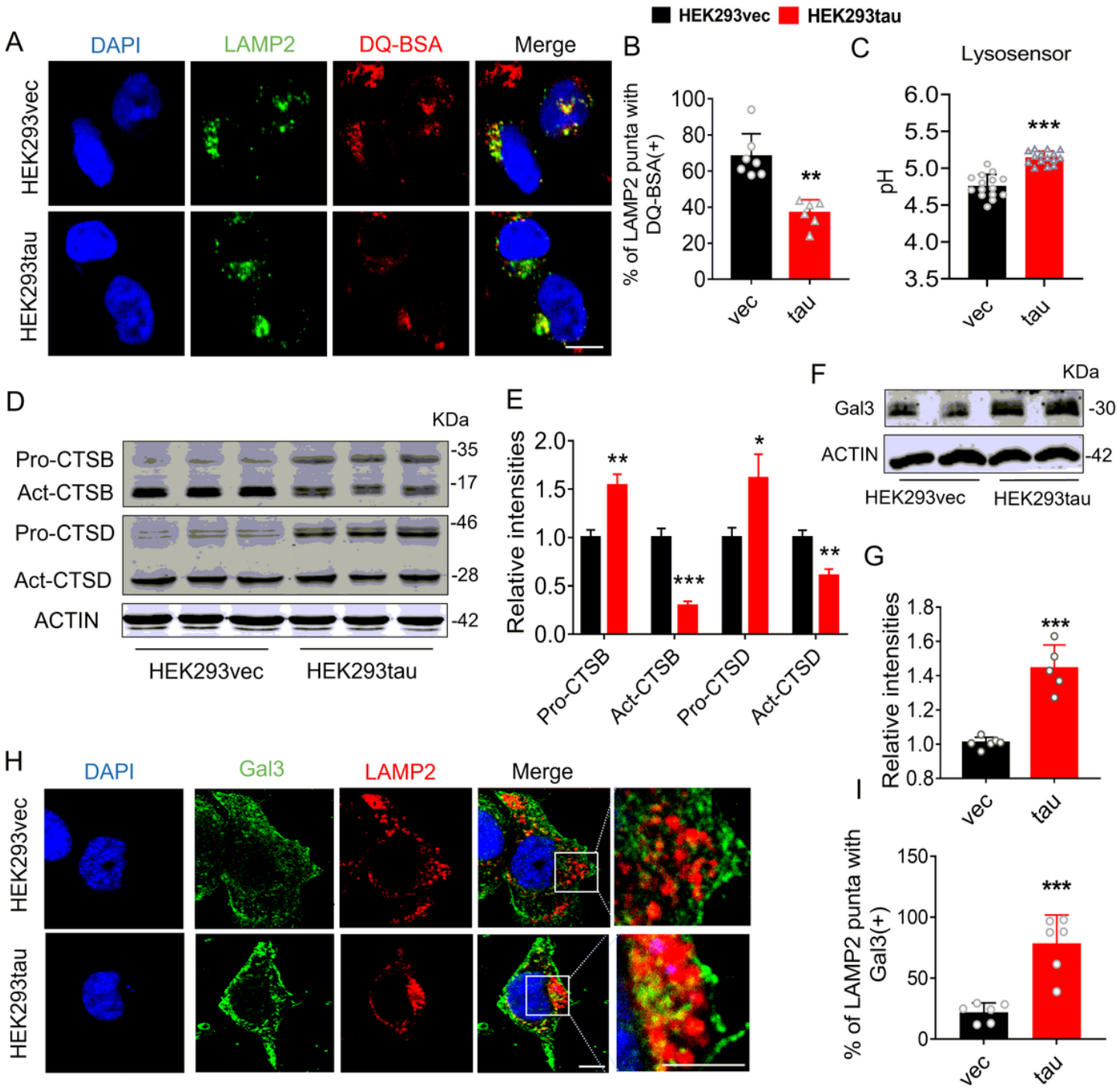

Figure 5

Legend not included with this version.

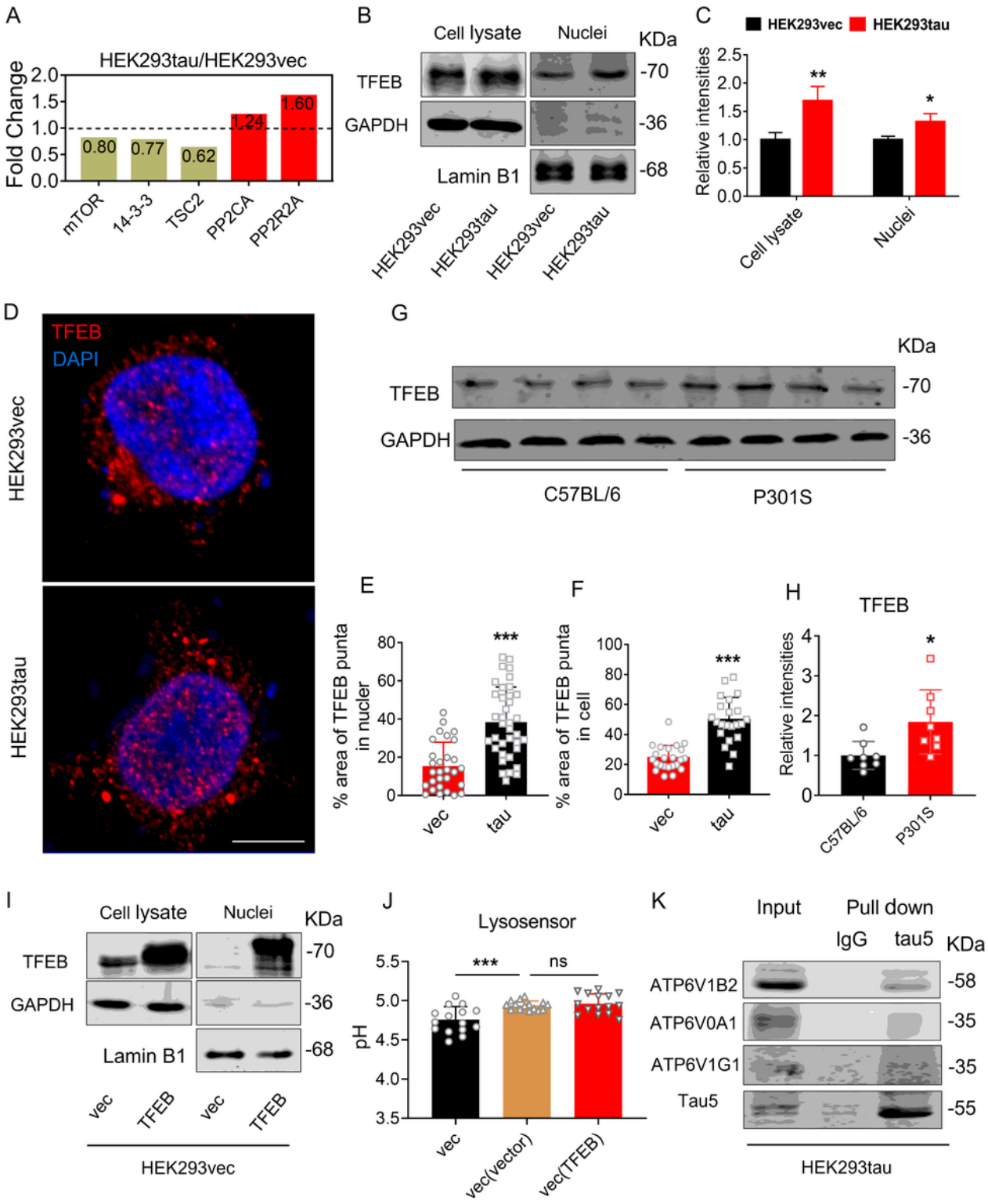

Figure 6

Legend not included with this version.